LA-UR- 00-4596

Approved for public release; distribution is unlimited.

Title: Some Recent Developments for Moving-Least-Squares Particle Methods

Author(s): Gary A Dilts

Submitted to: Proceedings

First MIT Conference on Computational Fluid and Solid Mechanics

June 12-14 2001, Cambridge MA

Los Alamos
NATIONAL LABORATORY

DISCLAIMER

DISCLAIMER

Portions of this document may be illegible in electronic image products. Images are produced from the best available original document.

Some Recent Developments for Moving-Least-Squares Particle Methods

Gary A. Dilts
September 27, 2000

Computer and Computational Sciences Division
Los Alamos National Laboratory
POB 1663, MS D413
Los Alamos NM 87544
gad@lanl.gov

Introduction

Dilts[1-2] has introduced an extension of smoothed-particle hydrodynamics (SPH)[3] using moving-least-squares interpolants[4] (MLSPH) that in certain variations provides linear completeness and improved tension stability at the cost of a loss of local conservation, or local flux balance. Local conservation has been found a highly desirable property of the original formulation of SPH[3]. Reference [2] also showed that local conservation could be regained satisfactorily at the cost of a loss of linear completeness, due to the inadequacy of the nodal quadrature scheme. In the course of regaining local conservation, it was found that it is necessary to introduce boundary conditions into the scheme in natural way, and that to do so required a means of identifying precisely which particles formed the boundary. A two-dimensional "exposure method" for doing so was introduced. We shall here describe a three-dimensional exposure method that performs to the same level of satisfaction.

Much effort was expended to achieve the simultaneous goals of local conservation and linear completeness via a suitable quadrature technique. If the ultimate answer has not been found yet, an interesting discovery has been made along the way regarding quadrature and MLS. We shall show that the MLS correction factors can be regarded in themselves as quadrature weights. A few examples will be given and some empirical observations related.

Three-Dimensional Boundary Detection

In the two-dimensional "exposure method", we draw a circle of radius h_i for each particle i, where h_i is the smoothing length of the kernel centered at particle i. For every neighbor circle j that intersects circle i we find the arc that circle j covers on circle i. If the union of the set of arcs from neighboring circles completely covers circle i, then particle i is an interior particle, otherwise it is a boundary particle. The coverage is determined by applying a quick sort to left endpoints of the arcs, and comparing the right endpoints of the sorted set. The boundary so determined is "exact" because in SPH, typically symmetrized kernels yield pair interactions that appear and disappear precisely when the radius-h circles touch or do not touch, respectively. The exposure method finds exactly those particles that are not completely bathed in interacting neighbors.

In extending the two-dimensional algorithm to three dimensions, a candidate *boundary circle* with a set of *surface arcs* created by intersections with neighboring circles is replaced by a candidate *boundary sphere* with a set of *surface circles* created by intersections with neighboring spheres. The chief idea is to apply the two-dimensional boundary detection scheme to the set of intersection circles on the surface of the candidate boundary particle. If any arc of an intersection circle is exposed, then the candidate is a boundary sphere. This criterion produces a boundary identification the same as would be determined by looking at the outer surface of a three-dimensional physical model of the particle configuration. The three-dimensional exposure method thus produces the exact solution to the problem. Figure 1 illustrates the basic idea. Figure 2 shows a cut-away of a time step from a ball-on-plate impact simulation where the three-dimensional exposure method has been applied. The method is more fully explained in reference [5].

Intrinsic Quadrature

Dolbow and Belytschko[6] present a detailed study of the quadrature of MLS shape functions in the context of the element-free Galerkin method[7], showing that accuracy depends on the relationship of the underlying background mesh to the supports of the MLS shape functions (particle configuration). In seeking Galerkin-based extensions of the original meshfree method SPH, as attempted in references [1] and [2], a convergent quadrature technique that does not require a background mesh is desirable in order to retain a fully meshfree character.

In reference [2] a nodal quadrature method given by

$$A_{ij} = \int \phi_i \nabla \phi_j \approx V_i \, \nabla_i \phi_j \tag{1}$$

was used, where V_i satisfies an evolution equation,

$$\dot{V}_i = V_i \sum_j v_j \nabla_i \phi_j \, , \tag{2}$$

and represents the evolving physical volume of the particle. The initial value of V_i is chosen to be the particle volume that is typically used for nodal quadrature, e.g. $\{h_i, \pi h_i^2, \frac{4}{3}\pi h_i^3\}$ in one, two, and three dimensions, respectively. This method is truly meshfree, but has several deficiencies. It is not anti-symmetric, does not lead to linear completeness, and does behave properly at boundaries. We focus in this paper on perhaps the most fundamental deficiency: it does not converge to the correct value except in special circumstances. We will show how to derive a one-point quadrature scheme that is convergent, and in the process, gain new insight into the nature of the moving-least-squares interpolant.

Recall the definition of the moving-least-squares (MLS) interpolants,

$$\begin{aligned}
&\phi_i(x) = p^T(x_i)\alpha(x)W_i(x), \\
&\alpha(x) = \left(\sum_k p(x_k)p^T(x_k)W_k(x)\right)^{-1} p(x), \\
&p(x) = [1, x, x^2, \ldots], \quad W_i(x) = \frac{N_i}{h_i^d} K\left(\frac{|x - x_i|}{h_i}\right).
\end{aligned} \tag{3}$$

The function K represents any real-valued function of the real line of compact support containing zero. The weight function W_i can be more general, but this definition is sufficient for this paper. Under the definitions $f_i \equiv f(x_i)$, $\nabla_i f \equiv \nabla f(x_i)$, and $c_i(x) \equiv p^T(x_i)\alpha(x)$ we have

$$\begin{aligned}
&W_{ij} = W_i(x_j), \quad c_{ij} = p_i^T \alpha_j, \quad \phi_{ij} = \phi_i(x_j) = c_{ij} W_{ij}, \\
&p_i \equiv \sum_j p_j \phi_{ji}, \quad \nabla_i p \equiv \sum_j p_j \nabla_i \phi_j, \\
&f_i \approx \sum_j f_j \phi_{ji}, \quad \nabla_i f \approx \sum_j f_j \nabla_i \phi_j,
\end{aligned} \tag{4}$$

where f is an arbitrary function.

We assume that W_i is of compact support and is normalized, thus representing an approximate delta function:

$$\int W_i = 1, \quad \int f(x)\, W_i(x)dx \approx f(x_i). \tag{5}$$

This implies that W_i has dimensions of inverse volume. Combining equations (4) and (5), we have

$$\int f(x)\, W_i(x)dx \approx \sum_k f_k\, W_{ki} c_{ki} \tag{6}$$

as an approximation for the integral of f against one of the W_i. If $W_{ki} = W_{ik}$ (which is true for the form specified in equations (3) and if $h_i = h_k$), then we have

$$\int f(x)\, W_i(x)dx \approx \sum_k f_k\, W_{ik} c_{ki}. \tag{7}$$

This implies that **the MLS correction factors $c_{ki} = p_k^T \alpha_i$, which have dimensions of volume, represent a set of quadrature weights for integration against the function W_i**. We now let f represent any of the components of p and observe by (4) that

$$p_i \equiv \sum_k p_k W_{ki} c_{ki}. \tag{8}$$

This leads to the interpretation that **the MLS correction factors $c_{ki} = p_k^T \alpha_i$ are precisely the quadrature weights that make the approximate quadrature scheme (6) exact for members of the MLS basis.**

To integrate an arbitrary function against an MLS basis function ϕ_i, we expand ϕ_i according to (3) and integrate the product $f(x)c_i(x)$ according to (6) to obtain

$$\int f\phi_i = \int f c_i W_i \approx \sum_k f_k c_{ik} c_{ki} W_{ki}. \qquad (10)$$

Setting $f(x) \equiv 1$ in (10), we have

$$\int \phi_i \approx \sum_k c_{ik} c_{ki} W_{ki}. \qquad (11)$$

To integrate an arbitrary function by itself, we can proceed two ways. First we expand $1 = \sum_i \phi_i$ and use (10) to obtain

$$\int f \approx \sum_j f_j q_j, \quad q_j = \sum_i c_{ij} c_{ji} W_{ji}. \qquad (12)$$

Secondly, we can expand $f \approx \sum_i f_i \phi_i$ and use (11) to obtain

$$\int f \approx \sum_j f_j q_j', \quad q_j' = \sum_i c_{ij} c_{ji} W_{ij}. \qquad (13)$$

If $W_{ji} = W_{ij}$, we have $q_j = q_j'$. We refer to the quadrature schemes represented by either (12) or (13) as *MLS intrinsic quadrature.*

Figure 3 illustrates the application of intrinsic quadrature (12) to the function $f(x) = \frac{1}{2}x + 2\sin\left(\frac{2\pi}{10}x\right)$. The function is plotted in Figure 3a. Particle configurations consisting of points and smoothing lengths given by

$$\begin{Bmatrix} x_i = (i + 0.2r_i)/(2^n \cdot 10) \\ h_i = h^*(1 + 0.2r_i)/(2^n \cdot 10) \end{Bmatrix}, \quad \begin{Bmatrix} i = \{0, \ldots, 2^n \cdot 10\} \\ n = \{0, \ldots, 4\} \end{Bmatrix}, \qquad (14)$$

where r_i is a random number between -1 and 1, were used. The randomness prevents a misleadingly optimistic assessment of the convergence rate. MLS is expensive, and only justified for highly non-uniform particle configurations. Convergence studies should therefore be conducted with non-uniform configurations. Figure 3b shows an example of a configuration given by (14) for $n = 0$ and $h^* = 1$. Figure 3c shows the quadrature weights given by (12) for this configuration and order-0 MLS interpolants ($p = [1]$ in (3)). Figure 3d and 3e show the base-10 logarithm of the maximum relative error of the nodal and intrinsic quadrature schemes, respectively. The convergence rate for nodal quadrature in this example is 0.935, while for intrinsic quadrature the rate is 1.56.

Figure 4 shows the configuration, weights and error norms for $n = 0$ and $h^* = 3$ and order-0 MLS. Note the increased smoothness of the weights. The correct value of the integral is 25. The nodal quadrature value at $n = 4$ was 75.6 and the convergence rate was 0.038. The intrinsic quadrature value at $n = 4$ was 25.4 and the convergence rate was 1.04. Nodal quadrature converges to 3 times the correct value, because it begins with an estimate of particle volume that is 3 times too large. If the average particle spacing happens to be the same as the average particle radius, then the nodal scheme converges to the correct value as in Figure 3. In general this is not the case and it cannot correct for arbitrary overlap of the particles. The intrinsic scheme on the other hand has the appropriate correction for overlap built in and converges to the correct value.

After studying many examples, a few empirical observations can be made. When the average smoothing length is equal to the average particle spacing, nodal quadrature will sometimes converge faster than intrinsic quadrature. On uniform configurations, intrinsic quadrature has been observed to converge super-linearly, when linear and higher-order MLS is used. On non-uniform configurations, order-0 MLS works as well as any higher-order version. On non-uniform configurations, there is no advantage to using higher-order

MLS. In fact, the convergence rate seems to fall off with the order of MLS interpolant used. Higher orders converge more slowly than lower orders. There appears to be no noticeable difference in performance between (12) and (13) when $W_{ij} \neq W_{ji}$.

Conclusions

A successful three-dimensional version of the two-dimensional boundary detection technique reported previously has been devised and implemented, providing an exact solution as did the two-dimensional version. Computational expense does not seem to be excessive, but could be improved.

The MLS correction factor has been discovered to provide a set of quadrature weights on scattered data points, and many examples demonstrate reasonable convergence. It is left to study the convergence with respect to variable smoothing length and fixed mesh, and develop an analytic theory to explain the observed inverse dependence of convergence rate on order of approximation.

Figures

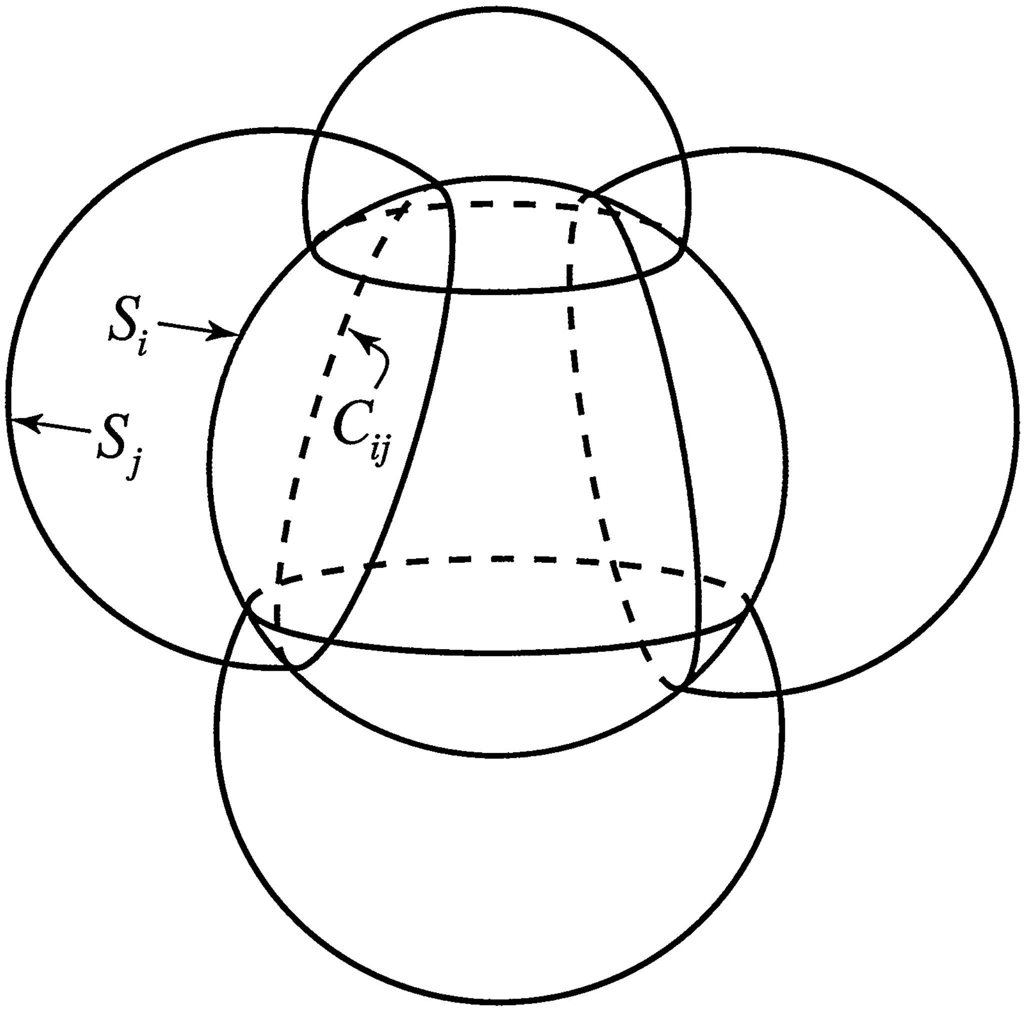

Figure 1. Green circle represents candidate boundary sphere. Black arcs represent portions of neighboring spheres. Circles of intersection are in blue. Red arcs are those portions of circles of intersection which are not covered. Any red arcs showing means particle is on boundary.

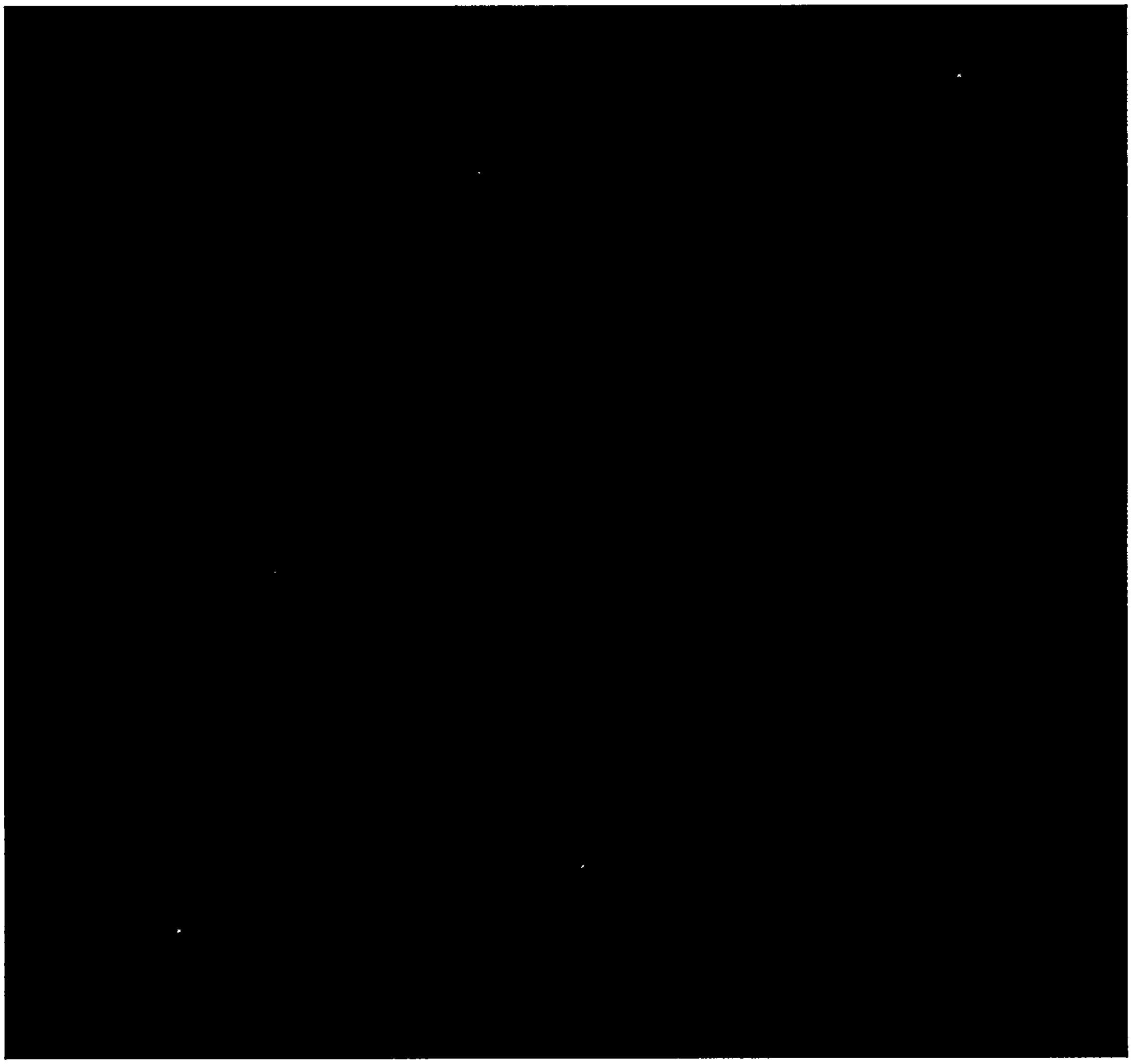

Figure 2. Cut-away of a time-step in a ball-on-plate impact simulation. Red spheres are boundary particles, blue spheres are interior particles.

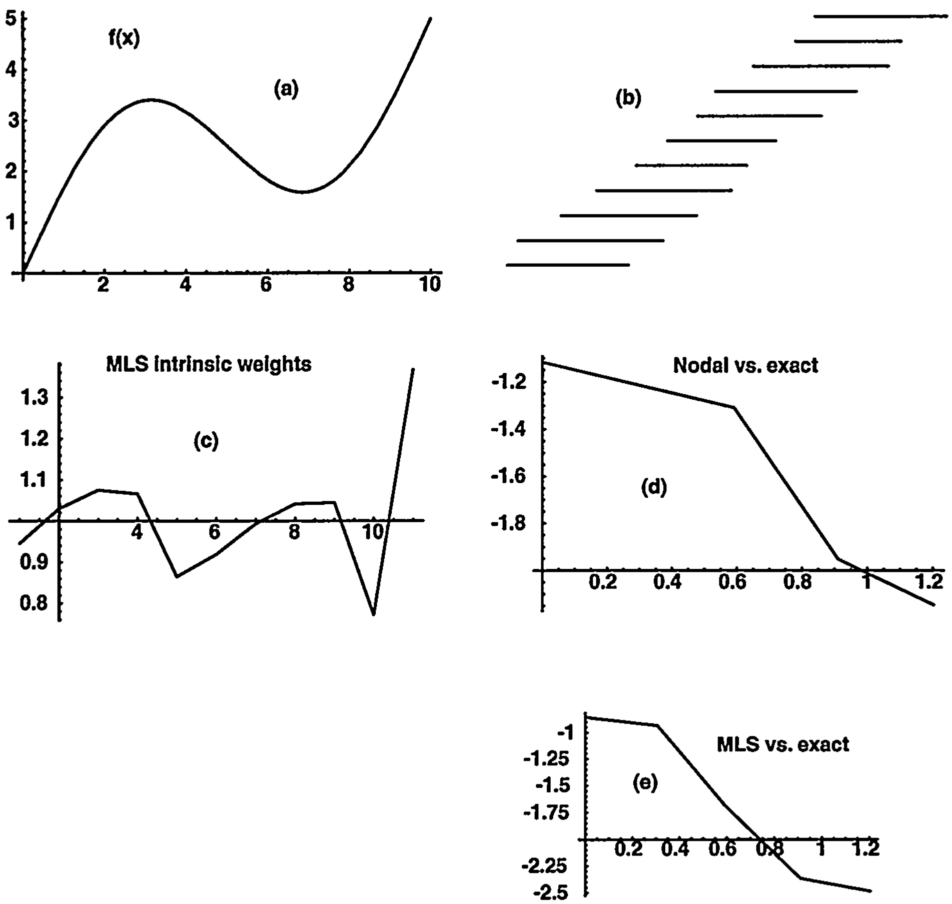

Figure 3 Convergence of nodal and intrinsic quadrature. (a) Sample function to integrate: $\frac{1}{2}x + 2\sin\left(\frac{2\pi}{10}x\right)$. (b) Initial randomized particle configuration. Lines plotted are from $(x_i - 2h_i, i)$ to $(x_i + 2h_i, i)$. (c) Quadrature weights corresponding to particle configuration (b) and order-0 MLS. (d) Log_{10} of maximum relative error for nodal quadrature for initial configuration plus four randomized refinements versus $-\log_{10}\max\{h_i\}$. (e) Log_{10} of maximum relative error for intrinsic quadrature for initial configuration plus four randomized refinements versus $-\log_{10}\max\{h_i\}$.

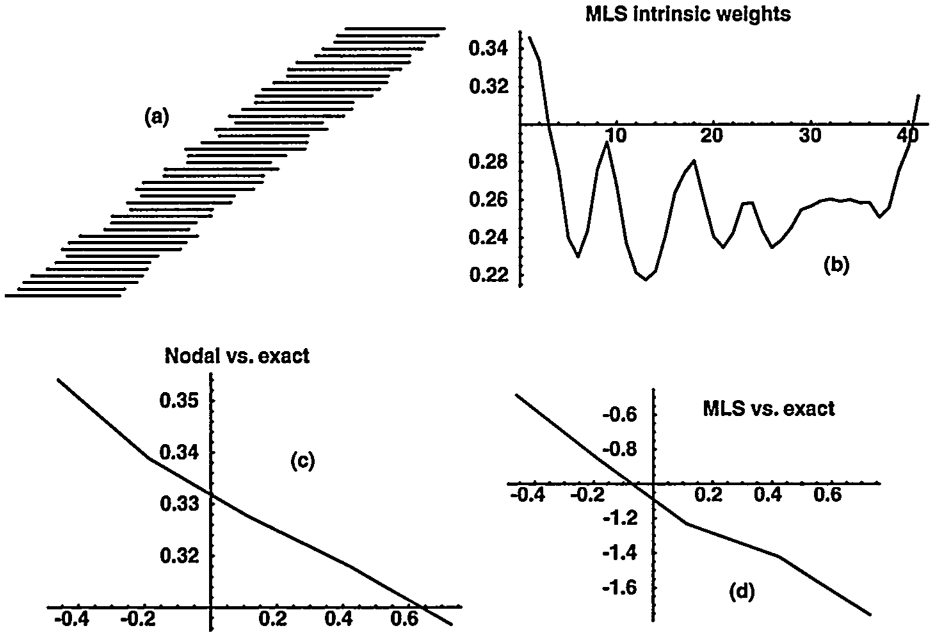

Figure 4. Convergence of nodal and intrinsic quadrature of same function used in . (a) Initial randomized particle configuration. Lines plotted are from $(x_i - 2h_i, i)$ to $(x_i + 2h_i, i)$. (b) Quadrature weights corresponding to particle configuration (a) and order-0 MLS. (c) Log_{10} of maximum relative error for nodal quadrature for initial configuration plus four randomized refinements versus $-\log_{10} \max\{h_i\}$. (d) Log_{10} of maximum relative error for intrinsic quadrature for initial configuration plus four randomized refinements versus $-\log_{10} \max\{h_i\}$.

---

[1] Dilts GA. Moving-least-squares-particle hydrodynamics: I. Consistency and stability. International journal for numerical methods in engineering mar 20, 1999. 44(8): 1115-1155

[2] Dilts GA. Moving least-squares particle hydrodynamics II: conservation and boundaries. International journal for numerical methods in engineering aug 10, 2000. 48(10): 1503

[3] Gingold RA, Monaghan JJ . Smoothed particle hydrodynamics: theory and application to non-spherical stars. Monthly notices of the royal astronomical society 1977. 181(2):375-389

[4] Lancaster P. and Salkauskas K. Surfaces Generated by Moving Least Squares Methods. Math. Comp. 1981. **37**:141-158

[5] Dilts GA and Haque AI. Three-Dimensional Boundary Detection for Smooth Particle Methods. submitted to Computer Methods in Applied Mechanics and Engineering. preprint at http://xdiv-lanl.gov/XHM/SPH/papers/boundary3d.pdf

[6] Dolbow J and Belytschko T. Numerical integration of the Galerkin weak form in meshfree methods. Computational mechanics 1999. 23(3):219-230

[7] T. Belytschko, Y.Y. Lu, and L. Gu. Element-Free Galerkin Methods. Int. J. Num. Meth. Eng. 1994. **37**:229-256